Coastal ocean acidification and increasing total alkalinity in the NW Mediterranean Sea

Lydia Kapsenberg[1], Samir Alliouane[1], Frédéric Gazeau[1], Laure Mousseau[1], and Jean-Pierre Gattuso[1,2,§]

[1]Sorbonne Universités, Université Pierre et Marie Curie-Paris 6, CNRS-INSU, Laboratoire d'Océanographie de Villefranche, 06230, Villefranche-sur-Mer, France

[2]Institute for Sustainable Development and International Relations, Sciences Po, 27 rue Saint Guillaume, F-75007 Paris, France

[§]Corresponding author

E-mail: gattuso@obs-vlfr.fr

Phone: +33 4 93 76 38 59

Abstract. Coastal time-series of ocean carbonate chemistry are critical for understanding how global anthropogenic change manifests in near-shore ecosystems. Yet, they are few and have low temporal resolution. At the time-series station Point B in the NW Mediterranean Sea, seawater was sampled weekly from 2007 through 2015, at 1 and 50 m, and analyzed for total dissolved inorganic carbon (C_T) and total alkalinity (A_T). Parameters of the carbonate system such as pH (pH_T, total hydrogen ion scale) were calculated and a deconvolution analysis was performed to identify drivers of change. The rate of surface ocean acidification was -0.0028 ± 0.0003 units pH_T yr^{-1}. This rate is larger than previously identified open-ocean trends due rapid warming that occurred over the study period (0.072 ± 0.022 °C yr^{-1}). The total pH_T change over the study period was of similar magnitude as the diel pH_T variability at this site. The acidification trend can be attributed to atmospheric carbon dioxide (CO_2) forcing (59 %, 2.08 ± 0.01 ppm CO_2 yr^{-1}) and warming (41 %). Similar trends were observed at 50 m but rates were generally slower. At 1 m depth, the increase in atmospheric CO_2 accounted for approximately 40 % of the observed increase in C_T (2.97 ± 0.20 μmol kg^{-1} yr^{-1}). The remaining increase in C_T may have been driven by the same unidentified process that caused an increase in A_T (2.08 ± 0.19 μmol kg^{-1} yr^{-1}). Based on the analysis of monthly trends, synchronous increases in C_T and A_T were fastest in the spring-summer transition. The driving process of the interannual increase in A_T has a seasonal and shallow component, which may indicate riverine or groundwater influence. This study exemplifies the importance of understanding changes in coastal carbonate chemistry through the lens of biogeochemical cycling at the land-sea interface. This is the first coastal acidification time-series providing multiyear data at high temporal resolution. The data confirm rapid warming in the Mediterranean Sea and demonstrate coastal acidification with a synchronous increase in total alkalinity.

Keywords – ocean change, ocean acidification, time-series, pH, alkalinity, dissolved inorganic carbon, pCO_2, Mediterranean Sea

1. Introduction

Maintaining time-series of oceanographic data is essential for understanding anthropogenic changes in the ocean (Tanhua et al., 2013). On land, fossil fuel burning, cement production, and land use changes have contributed ~600 Gt carbon to the atmosphere during the period 1750-2015 (Le Quéré et al., 2016). In the recent decade 2006-2015, an estimated 25 % of this anthropogenic carbon has been absorbed by the ocean in the form of carbon dioxide (CO_2; Le Quéré et al., 2016), and causing global changes to the ocean carbonate system. Absorption of CO_2 by seawater produces carbonic acid, which decreases seawater pH, and is of great concern for biological processes and marine ecosystems (Doney et al., 2009; Gattuso and Hansson, 2011; Pörtner et al., 2014). Since the preindustrial era, global mean ocean pH has declined by 0.1 (Rhein et al., 2013). Due to the declining trend of ocean pH with increasing anthropogenic CO_2, the process is termed 'ocean acidification', but this expression represents a suite of chemical changes, including increases in total dissolved inorganic carbon (C_T) and partial pressure of CO_2 (pCO_2) and decrease in calcium carbonate saturation states (Ω, aragonite and calcite; Dickson, 2010). Rates of ocean acidification differ by ocean region and range from -0.0026 (Irminger Sea, North Atlantic) to -0.0013 (South Pacific) units pH yr^{-1} (Bates et al., 2014). Such time-series remain spatially limited, especially in coastal regions, which provide valuable ecosystem services (Barbier et al., 2011; Costanza et al., 1997) and are under high anthropogenic impact (Halpern et al., 2008). Here, we present the first coastal ocean acidification time-series at high temporal resolution.

Compared to the global ocean, marginal seas serve a critical role in anthropogenic CO_2 storage via enhanced CO_2 uptake and export to the ocean interior (Lee et al., 2011). As a marginal sea, the Mediterranean Sea has a naturally high capacity to absorb but also buffer anthropogenic CO_2 (Álvarez et al., 2014; Palmiéri et al., 2015). This is primarily due to the high total alkalinity (A_T) of Mediterranean waters and overturning circulation (Lee et al.,

2011; Palmiéri et al., 2015; Schneider et al., 2010). In the Mediterranean Sea, the salinity-A_T relationship is driven by the addition of river discharge and Black Sea input, which are generally high in A_T (Copin-Montégut, 1993; Schneider et al., 2007). Combined with evaporation, this results in higher A_T and salinity in the Mediterranean Sea compared to the Atlantic Mediterranean source water (Jiang et al., 2014). On average, Mediterranean Sea A_T is 10 % higher than in the global ocean (Palmiéri et al., 2015). The surface ocean acidification rate, estimated at ΔpH_T (total hydrogen ion scale) of -0.08 since 1800, is comparable to that of the global ocean despite a 10 % greater anthropogenic carbon inventory (Palmiéri et al., 2015). Due to its important role in carbon sequestration and ecological sensitivity to anthropogenic change with economic consequences (Lacoue-Labarthe et al., 2016), the Mediterranean Sea could provide insight to global trends (Lejeusne et al., 2010).

Over the last few years, numerous studies have estimated ocean acidification rates across the Mediterranean Sea (Table 1). Together, these studies cover various study periods with a range of techniques yielding different results. For example, estimates of change in pH of bottom waters since the preindustrial era range between -0.005 to -0.06 (Palmiéri et al., 2015) and as much as -0.14 for full profile estimates (Touratier and Goyet, 2011). Techniques for estimating ocean acidification in the Mediterranean Sea thus far include: (1) hind-casting, using high-resolution regional circulation models (Palmiéri et al., 2015), the TrOCA approach as applied to cruise-based profile data (Krasakopoulou et al., 2011; Touratier and Goyet, 2011; Touratier et al., 2016) and others (Howes et al., 2015), (2) partially reconstructed time-series (Marcellin Yao et al., 2016), (3) comparative study periods (Luchetta et al., 2010; Meier et al., 2014), and (4) sensor-based observations over a short study period (Flecha et al., 2015). Ocean acidification time-series of consistent sampling over many years are lacking for the Mediterranean Sea (The MerMex Group et al., 2011),

90 particularly along the coast where river discharge influences the carbonate system (Ingrosso
91 et al., 2016).
92 Compared to the open ocean, shallow coastal sites exhibit natural variability in
93 carbonate chemistry over annual timeframes (Hofmann et al., 2011; Kapsenberg and
94 Hofmann, 2016; Kapsenberg et al., 2015), complicating the detection and relevance of open
95 ocean acidification in isolation of other processes (Duarte et al., 2013). In the NW Pacific
96 coast, rapid acidification of surface waters (ΔpH_T -0.058 units yr^{-1}) at Tatoosh Island was
97 documented in the absence of changes in known drivers of local pH variability (e.g.,
98 upwelling, eutrophication, and more; Wootton and Pfister, 2012; Wootton et al., 2008).
99 Further inshore, in the Hood Canal sub-basin of the Puget Sound, only 24-49 % of the
100 estimated pH decline from pre-industrial values could be attributed to anthropogenic CO_2
101 (Feely et al., 2010). The excess decrease in pH was attributed to increased remineralization
102 (Feely et al., 2010). Acidification rates documented along the North Sea Dutch coastline and
103 inlets were highly variable in space, with some exceeding the expected anthropogenic CO_2
104 rate by an order of magnitude while others exhibited an increase in pH (Provoost et al.,
105 2010).
106 Variability in coastal carbonate chemistry stems from both physical (e.g., upwelling,
107 river discharge; Feely et al., 2008; Vargas et al., 2016) and biological processes (e.g., primary
108 production, respiration, net calcification). Within watersheds, coastal carbonate chemistry is
109 affected by eutrophication (Borges and Gypens, 2010; Cai et al., 2011), groundwater supply
110 (Cai et al., 2003), and land use and rain influence on river alkalinity (Raymond and Cole,
111 2003; Stets et al., 2014). Over longer periods, pH can also be influenced by atmospheric
112 deposition (Omstedt et al., 2015). Through primary production and respiration, coastal
113 ecosystems produce pH fluctuations over hours (e.g., seagrass, kelp) to months (e.g.,
114 phytoplankton blooms; Kapsenberg and Hofmann, 2016). Due to existing pH variability in

115 coastal seas, it is necessary to quantify high-frequency trends in order to interpret the pH
116 changes inferred from lower-frequency sampling.
117 In this study, we present the first complete time-series data quantifying the present-
118 day ocean acidification rate for a coastal site in the Mediterranean Sea, based on weekly
119 measurements of A_T and C_T sampled from 2007 through 2015. For a subset of this time-
120 series, pH variability was documented using a SeaFET™ Ocean pH Sensor in order to assess
121 hourly pH variability. For comparison and consistency with other ocean acidification time-
122 series around the world, we report rates of change based on anomalies (Bates et al., 2014) and
123 identify drivers of change.
124
125 **2. Materials and methods**
126
127 **2.1. Site description**
128 A carbonate chemistry time-series was initiated in 2007 and maintained through 2015
129 in the NW Mediterranean Sea at the entrance of the Bay of Villefranche-sur-Mer, France
130 (Fig. 1): Point B station (43.686° N, 7.316° E, 85 m bottom depth). A second site,
131 Environment Observable Littoral buoy (EOL, 43.682° N, 7.319° E, 80 m bottom depth), was
132 used for pH sensor deployment starting in 2014. These two sites are 435 m apart. The site
133 Point B is an historical sampling point, since 1957, regarding several oceanographic
134 parameters. A full site description and research history has been detailed by De Carlo et al.
135 (2013). Briefly, the Bay is a narrow north-south facing inlet with steep bathymetry and
136 estimated volume of 310 million m^3. The surrounding region is predominately composed of
137 limestone with a series of shallow, submarine groundwater karst springs (Gilli, 1995). The
138 North current, a major and structuring counter-clockwise current in the Ligurian Sea, can
139 sometimes flow close to Point B. The Bay can also be, on occasion, influenced by local

countercurrents. Both of these hydrodynamics movements have signatures of river discharge. Limestone erosion can be observed in the A_T of rivers nearest to Point B (Paillon, due 4 km West; Var due 10 km West; and Roya due 26 km East). River A_T ranges between 1000 to 2000 µmol kg^{-1} (data from *Agence de l'Eau Rhône-Méditerranée-Corse*, http://sierm.eaurmc.fr), and is lower than seawater A_T. The Paillon River, whose plume on occasion reaches into the Bay (L. Mousseau, pers. obs.), was sampled on 18 August 2014 and had a A_T of 1585 ± 0.1 µmol kg^{-1} (N = 2, J.-P. Gattuso, unpubl.). Due to low primary productivity, seasonal warming drives the main annual variability in carbonate chemistry at this location (De Carlo et al., 2013).

2.2. Point B data collection, processing, and analysis

To document long-term changes in ocean carbonate chemistry at Point B, seawater was sampled weekly from 9 January 2007 to 22 December 2015. Samples were collected at 1 and 50 m, using a 12-L Niskin bottle at 9:00 local time. Seawater was transferred from the Niskin bottle to 500 mL borosilicate glass bottles and fixed within an hour via addition of saturated mercuric chloride for preservation of carbonate parameters, following recommendations by Dickson et al. (2007). Duplicate samples were collected for each depth. For each sampling event, CTD casts were performed either with a Seabird 25 or Seabird 25+ profiler whose sensors are calibrated at least every two years. Accuracy of conductivity (SBE4 sensor) and temperature (SBE3 sensor) measurements from CTD casts were 0.0003 S m^{-1} and 0.001°C, respectively.

Within six months of collection, bottle samples were analyzed for C_T and A_T via potentiometric titration following methods described by Edmond (1970) and DOE (1994), by *Service National d'Analyse des Paramètres Océaniques du CO_2*, at the Université Pierre et Marie Curie in Paris, France. Precision of C_T and A_T was less than 3 µmol kg^{-1}, and the

165 average accuracy was 2.6 and 3 µmol kg^{-1}, as compared with seawater certified reference
166 material (CRM) provided by A. Dickson (Scripps Institution of Oceanography). Only
167 obvious outliers were omitted from the analyses: three C_T values at 1 m (> 2300 µmol kg^{-1}),
168 one A_T value at 1 m (> 2900 µmol kg^{-1}), and one A_T value at 50 m (< 2500 µmol kg^{-1}). The
169 C_T and A_T measurements on replicate bottle samples were averaged for analyses.
170 Calculations of the carbonate system parameters were performed using the R package
171 seacarb version 3.1 with C_T, A_T, *in situ* temperature and salinity as inputs (Gattuso et al.,
172 2016). Total concentrations of silicate ($SiOH_4$) and phosphate (PO_4^{3-}) were used when
173 available from Point B (L. Mousseau, unpubl., http://somlit.epoc.u-bordeaux1.fr/fr/).
174 Detection limits for nutrients were 0.03 µM for $SiOH_4$ and 0.003 to 0.02 µM for PO_4^{3-};
175 relative precision of these analyses is 5-10 % (Aminot and Kérouel, 2007). Total boron
176 concentration was calculated from salinity using the global ratio determined by Lee et al.
177 (2010). The following constants were used: K_1 and K_2 from Lueker et al. (2000), K_f from
178 Perez and Fraga (1987), and K_s from Dickson (1990). Reported measured parameters are
179 temperature, salinity, A_T, and C_T, and derived parameters are pH_T (total hydrogen ion scale),
180 pH_T normalized to 25 ºC (pH_{T25}), pCO_2, and aragonite (Ω_a) and calcite (Ω_c) saturation states.
181 Salinity-normalized changes in A_T (nA_T) and C_T (nC_T) were calculated by dividing by *in situ*
182 salinity and multiplying by 38. Except for pH_{T25}, all parameters are reported at *in situ*
183 temperatures.
184 The average uncertainties of the derived carbonate parameters were calculated
185 according to the Gaussian method (Dickson and Riley, 1978) implemented in the "errors"
186 function of the R package seacarb 3.1 (Gattuso et al., 2016). The uncertainties are ± 2.7 x 10^{-10}
187 mol H^+ (about 0.015 units pH_T), ±15 µatm pCO_2, and ± 0.1 unit of the aragonite and calcite
188 saturation states.

To quantify interannual changes in carbonate parameters, the data were detrended for seasonality by subtracting the respective climatological monthly means computed for the period 2009-2015 from the time-series ('monthly means' from hereon). The resulting residuals were analyzed using a linear regression to compute anomaly trends. This approach follows methods from Bates et al. (2014) to allow for comparisons of trends observed at different time-series stations. All analyses were performed in R (R Core Team, 2016).

2.3. Deconvolution of pH_T and pCO_2

To identify proportional contributions of various drivers to ocean acidification trends at Point B, deconvolution of time-series pH_T and pCO_2 was performed following methods from García-Ibáñez et al. (2016) for observations at 1 and 50 m. The equation is described below for pH_T, where changes in pH_T are driven by changes in temperature (*T*), salinity (*S*), A_T, and C_T, over time (*t*), according to the following model:

$$\frac{dpH_T}{dt} = \frac{\partial pH_T}{\partial T}\frac{dT}{dt} + \frac{\partial pH_T}{\partial S}\frac{dS}{dt} + \frac{\partial pH_T}{\partial A_T}\frac{dA_T}{dt} + \frac{\partial pH_T}{\partial C_T}\frac{dC_T}{dt} \quad (1)$$

Here, $\frac{\partial pH_T}{\partial var}\frac{dvar}{dt}$ represents the slope contribution of changing *var* to the estimated change in pH_T ($\frac{dpH_T}{dt}$), where *var* is either temperature (T), salinity (S), A_T, or C_T. The sensitivity of pH to *var* ($\frac{\partial pH_T}{\partial var}$) was estimated by calculating pH_T using the true observations of *var* and holding the other three variables constant (mean value of the time-series) and regressing it to *var*. Sensitivity ($\frac{\partial pH_T}{\partial var}$) was then multiplied by the anomaly rate of *var* (Table 2). The calculation was repeated for pCO_2 ($\frac{dpCO_2}{dt}$) in order to compare the rate of increase with that of atmospheric CO_2.

As a sub-component of $\frac{\partial pCO_2}{\partial C_T}\frac{dC_T}{dt}$, the rate of anthropogenic CO_2 increase was estimated from atmospheric CO_2 concentrations nearest to Point B (Plateau Rosa, Italy,

courtesy of the World Data Center for Greenhouse Gases, http://ds.data.jma.go.jp/gmd/wdcgg/). For these data, missing daily values were linearly interpolated, monthly means were calculated and subtracted from the time-series to generate an anomaly time-series. A linear regression was performed on anomalies where the slope represents the rate of anthropogenic CO_2 increase in the atmosphere. Finally, to help identify different processes that might have contributed to the observed trends, linear regressions were performed on changes in A_T and C_T per month (mean value of observations within one month) from 2009 through 2015 and on the salinity-A_T relationship by year.

2.4. SeaFET data collection, processing, and analysis

To capture pH variability at higher-than-weekly sampling frequencies, a SeaFET™ Ocean pH sensor (Satlantic) was deployed on the EOL buoy (435 m from the Point B sampling site) starting in June 2014, at 2 m depth. Autonomous sampling was hourly and deployment periods ranged between 1 and 3 months. Field calibration samples for pH were collected weekly, using a Niskin bottle next to SeaFET within 15 min of measurement. This sampling scheme was sufficient for this site as there is no large high-frequency pH variability. Unlike Point B sampling, SeaFET calibration samples were processed for pH using the spectrophotometric method (Dickson et al., 2007) with purified m-cresol purple (purchased from the Byrne lab, University of South Florida). *In situ* temperature, salinity, and A_T measured at Point B, within 30 min of the SeaFET sampling, were used to calculate *in situ* pH_T of the calibration samples. SeaFET voltage was converted to pH_T using the respective calibration samples for each deployment period, following the methods and code described in Bresnahan et al. (2014) but adapted for use in R.

The estimated standard uncertainty in SeaFET pH_T is ± 0.01 and was calculated as the square root of the sum of each error squared. The sources of errors are: measurement error of

spectrophotometric pH (± 0.004, N = 68 mean SD of 5 replicate measurements per calibration sample for samples collected between 16 July 2014 and 3 May 2016), spatio-temporal mismatch sampling at EOL (± 0.007, mean offset of pH_T of the calibration samples from calibrated time-series), and variability in purified m-cresol dye batch accuracy as compared to Tris buffer CRM pH (± 0.006, mean offset of pH_T of the spectrophotometric measurement of Tris buffer from the CRM value).

3. Results

3.1. Time-series trends

At Point B from January 2007 to December 2015, more than 400 samples were collected for carbonate chemistry at both 1 and 50 m. Anomaly trends detected at 1 m (Fig. 2) were also significant at 50 m (Fig. 3, Table 2), with the exception that salinity increased at 50 m (0.0063 ± 0.0020 units yr^{-1}). At 1 m, trends were significant for pH_T (-0.0028 units yr^{-1}), A_T (2.08 µmol kg^{-1} yr^{-1}), C_T (2.97 µmol kg^{-1} yr^{-1}), pCO_2 (3.53 µatm yr^{-1}), and Ω_a (-0.0064 units yr^{-1}). At the same time, temperature anomaly increased (0.072 ºC yr^{-1}), but no significant change in the salinity was detected at 1 m. Trends of carbonate chemistry parameters were faster at 1 m compared to 50 m, with the exception of salinity and temperature. The warming rate at 50 m was slightly greater compared to 1 m, mostly due to increasing summer temperatures since 2007.

Strong seasonal cycles of carbonate chemistry parameters were present at Point B at 1 m (Fig. 4). Climatological monthly means (2007-2015) are described briefly and listed in Table S1. Mean temperature range was 11.2 ºC with a maximum at 24.77 ± 1.35 ºC in August and minimum of 13.58 ± 0.41 ºC in February. The range in A_T was 19 µmol kg^{-1} from June to September. The C_T range was 33 µmol kg^{-1} with a peak in late winter and minimum values in

August and October. Due to summer warming coinciding with the period of peak primary productivity (De Carlo et al. 2013), warming countered the influence of low C_T on pH. As a result, pH_T reached minimum values in summer (8.02 ± 0.03, July and August) and peaked in late winter (8.14 ± 0.01, February and March), for an overall annual pH range of 0.12. The corresponding pCO_2 range was 128 µatm from February to August. Seasonal cycles were smaller at 50 m compared to 1 m (Table S1).

3.2. Deconvolution of pH_T and pCO_2

Deconvolutions of pH and pCO_2 are presented in Table 3 and 4, respectively. The estimated anomaly trends ($\frac{dpH_T}{dt}$,$\frac{dpCO_2}{dt}$) from the deconvolution fall within the error of the observed anomaly trends (Table 2). The contribution of warming to the pH_T anomaly (-0.0011 units yr^{-1}, at 1 m) matched the difference between the trends of pH_T and pH_{T25C} (Table 2), which verifies that the deconvolution reproduced influences of temperature sensitivity well. Overall, these results indicate that the deconvolution analyses represent the observed trends well.

At both depths, the predominant driver of $\frac{dpH_T}{dt}$ and $\frac{dpCO_2}{dt}$ was the increase in C_T. Increasing A_T countered 66-69 and 60 % of the influence of increasing C_T on $\frac{dpH_T}{dt}$ and $\frac{dpCO_2}{dt}$, respectively. At 1 m, warming accounted for 41 and 37 % of $\frac{dpH_T}{dt}$ and $\frac{dpCO_2}{dt}$, respectively. Since warming was slightly greater at 50 m compared to 1 m, warming accounted for a larger proportional influence on $\frac{dpH_T}{dt}$ and $\frac{dpCO_2}{dt}$ at 50 m compared to 1 m. Increasing salinity at 50 m contributed slightly to $\frac{dpH_T}{dt}$ (4 %) and $\frac{dpCO_2}{dt}$ (2 %).

Atmospheric CO_2 anomaly at Plateau Rosa increased by 2.08 ± 0.01 ppm yr^{-1} ($F_{1,3285}$ = 4664, P <<0.001, R^2 0.93) during the study period 2007-2015, and represents the anthropogenic CO_2 forcing on seawater pH. To estimate the influence of anthropogenic CO_2

forcing at Point B, we assume air-sea CO_2 equilibrium (e.g., increase in atmospheric CO_2 causes an equal increase in seawater pCO_2) for the water mass at 1 m. This assumption is based on evidence that Point B is a weak sink for atmospheric CO_2 with near-balanced air-sea CO_2 flux on an annual time-frame (De Carlo et al., 2013). Considering the error associated with deconvolution of pCO_2 at 1 m, atmospheric CO_2 increase can, at most, represent 38-43 % of the total C_T contribution ($\frac{\partial pCO_2}{\partial C_T}\frac{dC_T}{dt}$) to $\frac{dpCO_2}{dt}$. This leaves 57-62 % of the total C_T contribution to pCO_2 trends unaccounted for.

As A_T is not influenced by addition of anthropogenic CO_2 to seawater but still increased, the next question was whether or not the changes in A_T and C_T were process-linked. At 1 m, regressions of annual monthly trends of A_T and C_T revealed similar seasonal cycles for both parameters (Fig. 5, Table S2). The fastest increases in A_T and C_T occurred from May through July. The smallest (non-significant) changes occurred in January. The synchronicity between monthly trends of A_T and C_T was also observed at 50 m, but the rates were slower (analysis not shown).

3.3. Salinity and A_T relationships

Over an annual observation period at 1 m, salinity was a poor predictor of A_T, with the exception of 2007 (Fig. 6). The R^2 value for each annual salinity-A_T relationship at 1 m ranged from 0.00 (in 2013) to 0.87 (in 2007) with y-intercepts (A_{T0}, total alkalinity of the freshwater end-member) ranging between -176 µmol kg^{-1} (in 2007) and 2586 µmol kg^{-1} (in 2013). The interannual variability of the salinity-A_T relationship was driven by the variability in A_T observed at salinity < 38.0 that was present from November through July.

Changes in salinity (based on monthly means) at Point B was small and ranged from 37.64 ± 0.26 to 38.21 ± 0.11 from May to September, following freshwater input in winter and spring and evaporation throughout summer and fall (Fig. 4). Highest (> 38.0) and most

311 stable salinity observations were made in August through October and coincided with the
312 period of maximum A_T (2562 and 2561 ± 9 µmol kg^{-1} in September and October,
313 respectively). Minimum A_T (2543 ± 14 µmol kg^{-1}) was observed in June, one month after
314 minimum salinity. To capture this seasonality without the inter-annual variation of A_T, the
315 salinity-A_T relationship at 1 m was estimated from climatological monthly means (cA_T and
316 *cS, N=12*) where cA_T units are µmol kg^{-1} and error terms are standard errors (R^2 = 0.74):

317 $$cA_T = 1554.9(\pm 185.9) + 26.3(\pm 4.9) \times cS \qquad (2)$$

318 At 50 m, monthly salinity and A_T were less correlated over an annual cycle (analysis not
319 shown). Salinity remained stable at 38.0 from January through September while A_T declined
320 by 13 µmol kg^{-1}. In general, seasonal changes were dampened at 50 m compared to 1 m.
321
322 **3.4. High-frequency pH data**
323 To verify the weekly sampling scheme at Point B, a continuous record of high-
324 frequency pH observations was obtained via11 consecutive SeaFET deployments from June
325 2014 to April 2016. Deployment periods averaged 58 ± 25 days with 5 ± 2 calibration
326 samples per deployment (Fig. 7). Only 5 % of the data was removed during quality control,
327 due to biofouling in one deployment and battery exhaustion in another, yielding 610 days of
328 data. The mean offset between calibration samples and the calibrated SeaFET pH time-series
329 was ± 0.007, indicating a high-quality pH dataset (Fig. 7c). Sensor data corroborated the
330 seasonal pH and temperature cycle observed at Point B (Fig. 7a-b). Event-scale effects (e.g.,
331 pH_T change ≥ 0.1 for days to weeks, *sensu* Kapsenberg and Hofmann 2016) were absent at
332 this site suggesting that weekly sampling was sufficient to describe seasonal and interannual
333 changes in carbonate chemistry at Point B. The magnitude of diel pH_T variability was small
334 (the 2.5th to 97.5th percentiles ranged between 0.01 and 0.05 units pH_T, Fig. 7d-e). Diel pH
335 variations increased from winter to spring with the greatest variability in April, May, and

June (ΔpH_T >0.035). The magnitude of pH variability was not correlated with temperature or the concentration of chlorophyll-a (data not shown).

4. Discussion

High resolution time-series are necessary to document coastal ocean acidification. At Point B in the NW coastal Mediterranean Sea, near-surface pH_T decreased by 0.0028 ± 0.0003 units yr^{-1}, based on weekly measurements from 2007 through 2015. Temperature increased by 0.072 ± 0.022 °C yr^{-1}. In addition, A_T increased by 2.08 ± 0.19 µmol kg^{-1} yr^{-1}, a change that is unrelated to direct effects of CO_2 absorption by seawater. In less than a decade, the total change in pH at Point B (ΔpH_T: 0.0252, Table 1) was of the same magnitude as the diel pH variability (ΔpH_T: 0.01-0.05) and $1/5^{th}$ of the magnitude of the seasonal pH cycle (ΔpH_T: 0.12) found at this site.

We can identify the drivers for the ocean acidification trends at Point B using the deconvolution of pH and pCO_2 and by assuming that the increase in A_T was due to increases in its carbon constituents, bicarbonate (HCO_3^-) and carbonate (CO_3^{2-}) ions. This assumption is based on the fact that (1) HCO_3^- and CO_3^{2-} ions together make up 96 % of A_T at Point B, (2) increases in HCO_3^- and CO_3^{2-} would both contribute to A_T and C_T and thereby explain the observed synchronicity of monthly trends in A_T and C_T (Fig. 5). Using the pCO_2 deconvolution, we can then sum the contributions to pCO_2 from A_T (-3.08 µatm pCO_2 yr^{-1}) and C_T (5.14 µatm pCO_2 yr^{-1}) trends to determine the proportional contribution of ΔC_T to ΔpCO_2 that is unrelated to changes in C_T brought on by A_T. This remaining 2.06 µatm pCO_2 yr^{-1} increase due to increasing C_T closely matched the magnitude of atmospheric CO_2 increase during the observation period (2.08 ± 0.01 ppm yr^{-1} at Plateau Rosa, Italy). The closeness of these numbers does not imply causation. However, given that surface waters at Point B exhibit a near-zero air-sea CO_2 flux over annual cycles (De Carlo et al., 2013), the

evidence supports the conclusion that the ocean acidification trend at Point B closely follows the rate of atmospheric CO_2 increase. The influence of atmospheric CO_2 can also be observed in the monthly changes in C_T. Monthly C_T trends are positive and statistically significant over more months than A_T trends (8 vs. 3 months), which are more seasonally restricted (Fig. 5).

Applying this simple model to pH_T, assuming changes in C_T are due to both increasing A_T (a neutralizing effect) and atmospheric CO_2 forcing, the surface ocean acidification trend at Point B can be attributed primarily to atmospheric CO_2 forcing (59 %) and secondarily to warming (41 %).

Using this same approach for observations at 50 m, the C_T contribution to pCO_2 trends that was unrelated to A_T change was 1.41 μatm pCO_2 yr^{-1}, which is 68 % of the rate of atmospheric CO_2 increase in contrast to 99 % at 1 m. Changes in pH_T can then be attributed to atmospheric CO_2 forcing (42 %), warming (54 %), and increasing salinity (3 %, which may result from warming). Due to slightly enhanced warming and reduced CO_2 penetration observed at 50 m, warming had a greater effect on the ocean acidification trend than atmospheric CO_2 forcing at depth compared to the surface.

The acidification rate at Point B (-0.0028 units pH_T yr^{-1}) is larger than those reported for other ocean time-series sites (-0.0026 to -0.0013 units pH yr^{-1}, Bates et al., 2014), likely due to differences in warming rates. The observed warming from 2007 through 2015 (0.72 to 0.88 ± 0.2 °C $decade^{-1}$) is extremely rapid relative to global trends in the upper 75 m from 1971 to 2010 (0.11 °C $decade^{-1}$, Rhein et al., 2013). The coastal region of Point B has warmed steadily since 1980 and with periods of rapid warming (Parravicini et al., 2015). Exacerbated warming may be related to the positive phases of the Atlantic Multi-decadal Oscillation (AMO) and North Atlantic Oscillation (NAO), both of which are associated with episodic warming of the Mediterranean Sea (Lejeusne et al., 2010). The AMO has been

385 positive since the 1990s[1] and positive NAO phases were prevalent during the second half of
386 our study[2].

387 Nearest to Point B, the acidification rate at DYFAMED, an open-sea site about 50 km
388 offshore from Point B (Fig. 1), was estimated at -0.003 ± 0.001 units pH_{SW} yr^{-1} from 1995 to
389 2011 (Marcellin Yao et al., 2016). At DYFAMED, warming contributed approximately 30 %
390 to the acidification rate and the remaining 70 % was attributed to anthropogenic CO_2
391 (Marcellin Yao et al., 2016). The uncertainty is large and makes direct comparison with Point
392 B unreliable but the results are agreeable. However, A_T at the DYFAMED did not change
393 significantly from 2007 through 2014 ($F_{1,51}$ 3.204, P = 0.0794, R^2 0.08, data from Coppola et
394 al., 2016). This may indicate that the processes driving changes in A_T at Point B are unique to
395 the coastal environment.

396 Similar changes in coastal carbonate chemistry were observed elsewhere in the near-
397 shore Mediterranean Sea. In the Northern Adriatic Sea, Luchetta et al. (2010) determined an
398 acidification rate in pH_T of -0.0025 yr^{-1} and an increase in A_T of 2.98 µmol kg^{-1} yr^{-1} at depths
399 shallower than 75 m, by comparing cruise data between the winters of 1983 and 2008. Point
400 B and Adriatic Sea observations are independent but reflect changes in seawater chemistry
401 that may be occurring across a wider coastal region. Additional time-series would help
402 resolve the spatial extent of the observed trends. Specifically, the Eastern Mediterranean Sea
403 would offer an important contrast, as pH of eastern waters is expected to be more sensitive to
404 atmospheric CO_2 addition due to their ability to absorb more anthropogenic CO_2 than either
405 the western Mediterranean or Atlantic waters (Álvarez et al., 2014).

406 While the trends in atmospheric CO_2 forcing and temperature account for the ocean
407 acidification trend, the increase in A_T and C_T increase beyond what can be attributed to

[1] http://www.cgd.ucar.edu/cas/catalog/climind/AMO.html
[2] http://www.cpc.ncep.noaa.gov/products/precip/CWlink/pna/month_nao_index.shtml

changes in atmospheric CO_2 was unexpected. The fastest increases in A_T and C_T occurred from May through July (Fig. 5), when the thermal stratification settles. In the NW Mediterranean, the main processes governing seasonal variability in A_T are evaporation increasing A_T in summer (i.e., June through September at Point B) and, to a lesser extent, phytoplankton uptake of nitrate (NO_3^-) and phosphate (PO_4^{3-}) increasing A_T from January through March (Cossarini et al., 2015). During the transition of these processes, salinity decreases to a minimum in May, reflecting freshwater input that dilutes A_T to minimum values at the start of summer. For C_T, peak values occur in winter when the water column is fully mixed. For reference, at DYFAMED, mixing occurs down to more than 2000 m depth and C_T is up to 100 µmol kg^{-1} higher in deep waters (Copin-Montégut and Bégovic, 2002). Notably, monthly trends of C_T at Point B were not statistically significant from November through January for the period 2007-2015. Following winter, C_T declines due to a combination of phytoplankton bloom carbon uptake and freshwater dilution (assuming river C_T < seawater C_T), until the onset of summer stratification. Summer warming leads to pCO_2 off-gassing to the atmosphere (De Carlo et al., 2013), thereby further decreasing C_T. The increases in A_T and C_T from 2007 through 2015 were more pronounced at 1 m compared to 50 m. This indicates that the process driving A_T and C_T trends are stronger at the surface and affect carbonate chemistry primarily during the spring-summer transition from May through July.

While the drivers of ocean acidification trends are identified and quantified above, the increase in A_T and increase in C_T beyond what can be attributed to changes in atmospheric CO_2 requires some speculation. Some biogeochemical processes can be ruled out as drivers. For example, changes in benthic processes are very unlikely. Reduced calcium carbonate ($CaCO_3$) precipitation rates would increase A_T but would increase C_T. Even so, the dominant ecosystem in the Bay of Villefranche-sur-Mer is seagrass meadows, which harbor relatively

few calcifying organisms. Dissolution of calcium carbonate sediment would contribute to A_T and C_T increase in the water column. However, as the water was supersaturated with respect to both aragonite and calcite, this could only be mediated by biological processes. Carbonate dissolution following CO_2 production via oxic degradation of organic matter releases A_T and C_T in a 1:1 ratio (Moulin et al., 1985). Likewise, anaerobic remineralization produces alkalinity (Cai et al., 2011). In the sediment of the Bay of Villefranche, sulfate reduction coupled with precipitation of sulfide minerals is the dominant anoxic mineralization pathway (Gaillard et al., 1989). An increase in these processes would explain the observed increase in A_T and C_T, but as trends were slower at 50 m compared to 1 m, this would suggest the dominance of a process taking place in surface waters.

In the upper water column at Point B, changes in biological processes are unlikely to explain the observed trends in A_T and C_T. For example, the concentration of chlorophyll-a, a proxy of primary production, has decreased since 1995, nutrients increased, and phytoplankton blooms have shifted towards earlier dates in the year (Irisson et al., 2012). While a decrease in net primary production could drive C_T trends, the observed increase in NO_3^- and PO_4^{3-} would cause a small decrease in A_T (Wolf-Gladrow et al., 2007). Stimulated community respiration could result from warming waters but enhanced remineralization would cause a decrease in A_T (Wolf-Gladrow et al., 2007).

The lack of salinity change at the surface excludes additional processes as drivers of A_T and C_T increase at Point B. For example, increased summertime evaporation (concentration effect) and reduced freshwater input (decreased dilution effect) would both be expected to cause an increase in salinity, which was not observed. Increased input of Eastern Mediterranean Sea waters could increase A_T, but this is unlikely as this water mass flows much deeper than Point B (Millot and Taupier-Letage, 2005).

457 Instead, the observed changes in A_T and C_T could be due to increased limestone
458 weathering which would increase the input of A_T from land to the sea via rivers and
459 groundwater. Rivers contribute both A_T and C_T to the Mediterranean Sea (Copin-Montégut,
460 1993; Tamše et al., 2015). River A_T originates from erosion and is correlated with bedrock
461 composition (e.g., McGrath et al., 2016). Positive trends in river A_T have been documented in
462 North America and occur via a number of processes including: (1) the interplay of rainfall
463 and land-use (Raymond and Cole, 2003), (2) anthropogenic limestone addition (a.k.a.,
464 liming) used to enhance agriculture soil pH (Oh and Raymond, 2006; Stets et al., 2014) and
465 freshwater pH (Clair and Hindar, 2005), and (3) potentially indirect effects of anthropogenic
466 CO_2 on groundwater CO_2-acidification and weathering (Macpherson et al., 2008). Such, and
467 other, processes were hypothesized to have driven A_T changes in the Baltic Sea (Müller et al.,
468 2016). There, an increase in A_T of 3.4 µmol kg^{-1} yr^{-1} was observed from 1995 to 2014 (mean
469 salinity = 7). In contrast to Point B, the increase in Baltic Sea A_T was not noticeable at
470 salinity > 30 (Müller et al., 2016).
471 Given the above speculations, the simplest plausible mechanisms causing the
472 unexpected A_T and C_T trends would be through increasing A_T of the freshwater end-member
473 of Point B. Local precipitation, however, did not have an influential effect and was not
474 correlated with salinity or A_T (Fig. S1). While submarine groundwater springs can be a
475 significant source of nutrients, A_T, and C_T to the ocean (Cai et al., 2003; Slomp and Van
476 Cappellen, 2004), carbonate chemistry contributions of local submarine springs are currently
477 unknown (Gilli, 1995). Signatures of limestone erosion can be observed in A_T of nearby
478 rivers (Var, Paillon, and Roya) but detailed time-series are not available. Likewise, riverine
479 influence at Point B has not been quantified. If river runoff exerts a dominant control on
480 Point B carbonate chemistry, there is a lag effect, as freshwater influence peaked in May but
481 A_T and C_T increased fastest from May through July. Consequently, this hypothesis needs

further investigation. Until the source of A_T increase is properly identified, use of this observation in modeling should be implemented with caution.

5. Conclusion

Predictions of coastal ocean acidification remain challenging due the complexity of biogeochemical processes occurring at the ocean-land boundary. At the Point B coastal monitoring station in the NW Mediterranean Sea, surface ocean acidification was due to atmospheric CO_2 forcing and rapid warming over the observation period 2007-2015. However, additional trends in A_T and C_T were observed and remain unexplained, but these trends could relate to riverine and groundwater input. The influence of a coastal boundary processes influencing seawater A_T and C_T presents a potentially major difference between coastal and offshore changes in ocean chemistry. This study highlights the importance of considering other anthropogenic influences in the greater land-sea region that may contribute to coastal biogeochemical cycles (*sensu* Duarte et al. 2013) and alter projections of anthropogenic change in near-shore waters.

Data availability – Time-series data from Point B are available at Pangaea® (doi: 10.1594/PANGAEA.727120)

Author contribution – JPG initiated the study, LM supervised data collection, SA performed SeaFET deployments and calibration, JPG and LK designed and JPG conducted statistical analyses, and LK prepared the manuscript with contributions from all authors.

Competing interests - The authors declare that they have no conflict of interest.

Acknowledgements – Thanks are due to the Service d'Observation Rade de Villefranche (SO-Rade) of the Observatoire Océanologique and the Service d'Observation en Milieu Littoral (SOMLIT/CNRS-INSU) for their kind permission to use the Point B data. Discrete samples were analyzed for C_T and A_T by the *Service National d'Analyse des Paramètres Océaniques du CO2*. The authors thank Jean-Yves Carval, Anne-Marie Corre, Maïa Durozier, Ornella Passafiume and Frank Petit for sampling assistance, to Steeve Comeau and Alice Webb for help with data analysis, and to Bernard Gentili for producing Fig. 1. Atmospheric CO_2 data from Plateau Rosa was collected by Ricerca sul Sistema Energetico (RSE S.p.A.); we are grateful for their contribution. We acknowledge L. Coppola for providing DYFAMED data (Coppola et al., 2016) and Météo-France for supplying the meteorological data and the HyMeX database teams (ESPRI/IPSL and SEDOO/Observatoire Midi-Pyrenees) for their help in accessing them. The *Agence de l'Eau Rhône-Méditerranée-Corse* kindly provided data on the chemistry of local rivers. Alexandre Dano, Gilles Dandec and Dominique Chassagne provided the high-resolution bathymetric data for the volume estimate of the Bay. We are grateful for helpful comments from Nicolas Metzl on the manuscript and those from two anonymous reviewers. This work is a contribution to the European Project on Ocean Acidification (EPOCA; contract # 211384) and the MedSeA project (contract # 265103), which received funding from the European Community's Seventh Framework Programme, and to the United States National Science Foundation Ocean Sciences Postdoctoral Research Fellowship (OCE-1521597) awarded to LK.

References

Álvarez, M., Sanleón-Bartolomé, H., Tanhua, T., Mintrop, L., Luchetta, A., Cantoni, C., Schroeder, K., and Civitarese, G.: The CO_2 system in the Mediterranean Sea: a basin wide perspective, Ocean Sci., 10, 69-92, 10.5194/os-10-69-2014, 2014.

Aminot, A., and Kérouel, R.: Dosage automatique des nutriments dans les eaux marines: méthodes d'analyse en milieu marin, edited by: Ifremer, 188 pp., 2007.

Barbier, E. B., Hacker, S. D., Kennedy, C., Koch, E. W., Stier, A. C., and Silliman, B. R.: The value of estuarine and coastal ecosystem services, Ecol. Monogr., 81, 169-193, 10.1890/10-1510.1, 2011.

Bates, N. R., Astor, Y. M., Church, M. J., Currie, K., Dore, J. E., González-Dávila, M., Lorenzoni, L., Muller-Karger, F., Olafsson, J., and Santana-Casiano, J. M.: A time-series view of changing ocean chemistry due to ocean uptake of anthropogenic CO_2 and ocean acidification, Oceanography, 27, 126-141, 2014.

Borges, A. V., and Gypens, N.: Carbonate chemistry in the coastal zone responds more strongly to eutrophication than ocean acidification, Limnol. Oceanogr., 55, 346-353, 10.4319/lo.2010.55.1.0346, 2010.

Bresnahan, P. J., Martz, T. R., Takeshita, Y., Johnson, K. S., and LaShomb, M.: Best practices for autonomous measurement of seawater pH with the Honeywell Durafet, Methods Oceangr., 9, 44-60, 2014.

Cai, W.-J., Wang, Y., Krest, J., and Moore, W. S.: The geochemistry of dissolved inorganic carbon in a surficial groundwater aquifer in North Inlet, South Carolina, and the carbon fluxes to the coastal ocean, Geochim. Cosmochim. Acta, 67, 631-639, 10.1016/S0016-7037(02)01167-5, 2003.

Cai, W.-J., Hu, X., Huang, W.-J., Murrell, M. C., Lehrter, J. C., Lohrenz, S. E., Chou, W.-C., Zhai, W., Hollibaugh, J. T., Wang, Y., Zhao, P., Guo, X., Gundersen, K., Dai, M., and Gong, G.-C.: Acidification of subsurface coastal waters enhanced by eutrophication, Nat. Geosci., 4, 766-770, 10.1038/ngeo1297, 2011.

Clair, T. A., and Hindar, A.: Liming for the mitigation of acid rain effects in freshwaters: a review of recent results, Environ. Rev., 13, 91-128, 10.1139/a05-009, 2005.

557 Copin-Montégut, C.: Alkalinity and carbon budgets in the Mediterranean Sea, Global
558 Biogeochem. Cycles, 7, 915-925, 10.1029/93GB01826, 1993.
559 Copin-Montégut, C., and Bégovic, M.: Distributions of carbonate properties and oxygen
560 along the water column (0–2000 m) in the central part of the NW Mediterranean Sea
561 (Dyfamed site): influence of winter vertical mixing on air–sea CO_2 and O_2 exchanges,
562 Deep-Sea Res. II, 49, 2049-2066, 10.1016/S0967-0645(02)00027-9, 2002.
563 Coppola, L., Diamond Riquier, E., and Carval, T.: Dyfamed observatory data, SEANOE,
564 10.17882/43749, 2016.
565 Cossarini, G., Lazzari, P., and Solidoro, C.: Spatiotemporal variability of alkalinity in the
566 Mediterranean Sea, Biogeosciences, 12, 1647-1658, 10.5194/bg-12-1647-2015, 2015.
567 Costanza, R., d'Arge, R., de Groot, R., Farber, S., Grasso, M., Hannon, B., Limburg, K.,
568 Naeem, S., O'Neill, R. V., Paruelo, J., Raskin, R. G., Sutton, P., and van den Belt, M.:
569 The value of the world's ecosystem services and natural capital, Nature, 387, 253-260,
570 1997.
571 De Carlo, E. H., Mousseau, L., Passafiume, O., Drupp, P. S., and Gattuso, J.-P.: Carbonate
572 chemistry and air–sea CO_2 flux in a NW Mediterranean bay over a four-year period:
573 2007–2011, Aquatic Geochemistry, 19, 399-442, 10.1007/s10498-013-9217-4, 2013.
574 Dickson, A.: The carbon dioxide system in seawater: equilibrium chemistry and
575 measurements, in: Guide to best practices for ocean acidification research and data
576 reporting, edited by: Fabry, V. J., Hansson, L., and Gattuso, J.-P., Luxembourg:
577 Publications Office of the European Union, 17-40, 2010.
578 Dickson, A. G., and Riley, J. P.: The effect of analytical error on the evaluation of the
579 components of the aquatic carbon-dioxide system, Mar. Chem., 6, 77-85, 10.1016/0304-
580 4203(78)90008-7, 1978.

Dickson, A. G.: Standard potential of the reaction: AgCl(s) + 1/2 H_2(g) = Ag(s) + HCl(aq), and and the standard acidity constant of the ion HSO_4^- in synthetic sea water from 273.15 to 318.15 K, The Journal of Chemical Thermodynamics, 22, 113-127, 10.1016/0021-9614(90)90074-Z, 1990.

Dickson, A. G., Sabine, C. L., and Christian, J. R.: Guide to best practices for ocean CO_2 measurements, PICES Special Publication, 3, 191 pp., 2007.

DOE: Handbook of methods for the analysis of the various parameters of the carbon dioxide system in sea water, Carbon Dioxide Information Analysis Center, Oak Ridge National Laboratory, 1994.

Doney, S. C., Fabry, V. J., Feely, R. A., and Kleypas, J. A.: Ocean acidification: the other CO_2 problem, Ann. Rev. Mar. Sci., 1, 169-192, 10.1146/annurev.marine.010908.163834, 2009.

Duarte, C. M., Hendriks, I. E., Moore, T. S., Olsen, Y. S., Steckbauer, A., Ramajo, L., Carstensen, J., Trotter, J. A., and McCulloch, M.: Is ocean acidification an open-ocean syndrome? Understanding anthropogenic impacts on seawater pH, Estuaries and Coasts, 36, 221-236, 10.1007/s12237-013-9594-3, 2013.

Edmond, J. M.: High precision determination of titration alkalinity and total carbon dioxide content of sea water by potentiometric titration, Deep-Sea Research, 17, 737-750, 10.1016/0011-7471(70)90038-0, 1970.

Feely, R. A., Sabine, C. L., Hernandez-Ayon, J. M., Ianson, D., and Hales, B.: Evidence for upwelling of corrosive "acidified" water onto the continental shelf, Science, 320, 1490-1492, 10.1126/science.1155676, 2008.

Feely, R. A., Alin, S. R., Newton, J., Sabine, C. L., Warner, M., Devol, A., Krembs, C., and Maloy, C.: The combined effects of ocean acidification, mixing, and respiration on pH

and carbonate saturation in an urbanized estuary, Estuar. Coast. Shelf Sci., 88, 10.1016/j.ecss.2010.05.004, 2010.

Flecha, S., Pérez, F. F., García-Lafuente, J., Sammartino, S., Ríos, A. F., and Huertas, I. E.: Trends of pH decrease in the Mediterranean Sea through high frequency observational data: indication of ocean acidification in the basin, Sci. Rep., 5, 16770, 10.1038/srep16770, 2015.

Gaillard, J.-F., Pauwels, H., and Michard, G.: Chemical diagenesis in coastal marine sediments, Oceanol. Acta, 12, 175-187, 1989.

García-Ibáñez, M. I., Zunino, P., Fröb, F., Carracedo, L. I., Ríos, A. F., Mercier, H., Olsen, A., and Pérez, F. F.: Ocean acidification in the subpolar North Atlantic: rates and mechanisms controlling pH changes, Biogeosciences, 13, 3701-3715, 10.5194/bg-13-3701-2016, 2016.

Gattuso, J.-P., Epitalon, J.-M., and Lavigne, H.: seacarb: Seawater Carbonate Chemistry. R package version 3.1.1 https://cran.r-project.org/package=seacarb, 2016.

Gattuso, J. P., and Hansson, L.: Ocean acidification, Oxford University Press, Oxford, 2011.

Gilli, E.: Etude des sources karstiques sous-marines et littorales des Alpes Maritimes entre Menton et Nice, 41, 1995.

Halpern, B. S., Walbridge, S., Selkoe, K. A., Kappel, C. V., Micheli, F., D'Agrosa, C., Bruno, J. F., Casey, K. S., Ebert, C., and Fox, H. E.: A global map of human impact on marine ecosystems, Science, 319, 948-952, 2008.

Hofmann, G. E., Smith, J. E., Johnson, K. S., Send, U., Levin, L. A., Micheli, F., Paytan, A., Price, N. N., Peterson, B., Takeshita, Y., Matson, P. G., Crook, E. D., Kroeker, K. J., Gambi, M. C., Rivest, E. B., Frieder, C. A., Yu, P. C., and Martz, T. R.: High-frequency dynamics of ocean pH: a multi-ecosystem comparison, PLoS One, 6, e28983, 10.1371/journal.pone.0028983, 2011.

630 Howes, E. L., Stemmann, L., Assailly, C., Irisson, J. O., Dima, M., Bijma, J., and Gattuso, J.
631 P.: Pteropod time series from the North Western Mediterranean (1967-2003): impacts of
632 pH and climate variability, Mar. Ecol. Prog. Ser., 531, 193-206, 2015.
633 Ingrosso, G., Giani, M., Comici, C., Kralj, M., Piacentino, S., De Vittor, C., and Del Negro,
634 P.: Drivers of the carbonate system seasonal variations in a Mediterranean gulf, Estuar.
635 Coast. Shelf Sci., 168, 58-70, 10.1016/j.ecss.2015.11.001, 2016.
636 Irisson, J.-O., Webb, A., Passafiume, O., and Mousseau, L.: Detecting hydrologic variations
637 in a long term monitoring time series, Europole Mer Gordon-like conference "Time-series
638 analysis in marine science and application for industry", Brest, France, 17-21 Sept 2012,
639 2012.
640 Jiang, Z.-P., Tyrrell, T., Hydes, D. J., Dai, M., and Hartman, S. E.: Variability of alkalinity
641 and the alkalinity-salinity relationship in the tropical and subtropical surface ocean,
642 Global Biogeochem. Cycles, 28, 729-742, 10.1002/2013GB004678, 2014.
643 Kapsenberg, L., Kelley, A. L., Shaw, E. C., Martz, T. R., and Hofmann, G. E.: Near-shore
644 Antarctic pH variability has implications for biological adaptation to ocean acidification,
645 Sci. Rep., 5, 9638, 10.1038/srep09638, 2015.
646 Kapsenberg, L., and Hofmann, G. E.: Ocean pH time-series and drivers of variability along
647 the northern Channel Islands, California, USA, Limnol. Oceanogr., 61, 953-968,
648 10.1002/lno.10264, 2016.
649 Krasakopoulou, E., Souvermezoglou, E., and Goyet, C.: Anthropogenic CO_2 fluxes in the
650 Otranto Strait (E. Mediterranean) in February 1995, Deep-Sea Res. I, 58, 1103-1114,
651 10.1016/j.dsr.2011.08.008, 2011.
652 Lacoue-Labarthe, T., Nunes, P. A. L. D., Ziveri, P., Cinar, M., Gazeau, F., Hall-Spencer, J.
653 M., Hilmi, N., Moschella, P., Safa, A., Sauzade, D., and Turley, C.: Impacts of ocean

654 acidification in a warming Mediterranean Sea: An overview, Regional Studies in Marine
655 Science, 5, 1-11, 10.1016/j.rsma.2015.12.005, 2016.
656 Le Quéré, C., Andrew, R. M., Canadell, J. G., Sitch, S., Korsbakken, J. I., Peters, G. P.,
657 Manning, A. C., Boden, T. A., Tans, P. P., Houghton, R. A., Keeling, R. F., Alin, S.,
658 Andrews, O. D., Anthoni, P., Barbero, L., Bopp, L., Chevallier, F., Chini, L. P., Ciais, P.,
659 Currie, K., Delire, C., Doney, S. C., Friedlingstein, P., Gkritzalis, T., Harris, I., Hauck, J.,
660 Haverd, V., Hoppema, M., Klein Goldewijk, K., Jain, A. K., Kato, E., Körtzinger, A.,
661 Landschützer, P., Lefèvre, N., Lenton, A., Lienert, S., Lombardozzi, D., Melton, J. R.,
662 Metzl, N., Millero, F., Monteiro, P. M. S., Munro, D. R., Nabel, J. E. M. S., Nakaoka, S.
663 I., O'Brien, K., Olsen, A., Omar, A. M., Ono, T., Pierrot, D., Poulter, B., Rödenbeck, C.,
664 Salisbury, J., Schuster, U., Schwinger, J., Séférian, R., Skjelvan, I., Stocker, B. D.,
665 Sutton, A. J., Takahashi, T., Tian, H., Tilbrook, B., van der Laan-Luijkx, I. T., van der
666 Werf, G. R., Viovy, N., Walker, A. P., Wiltshire, A. J., and Zaehle, S.: Global Carbon
667 Budget 2016, Earth Syst. Sci. Data, 8, 605-649, 10.5194/essd-8-605-2016, 2016.
668 Lee, K., Kim, T.-W., Byrne, R. H., Millero, F. J., Feely, R. A., and Liu, Y.-M.: The universal
669 ratio of boron to chlorinity for the North Pacific and North Atlantic oceans, Geochim.
670 Cosmochim. Acta, 74, 1801-1811, 10.1016/j.gca.2009.12.027, 2010.
671 Lee, K., Sabine, C. L., Tanhua, T., Kim, T.-W., Feely, R. A., and Kim, H.-C.: Roles of
672 marginal seas in absorbing and storing fossil fuel CO_2, Energy & Environmental Science,
673 4, 1133-1146, 10.1039/C0EE00663G, 2011.
674 Lejeusne, C., Chevaldonné, P., Pergent-Martini, C., Boudouresque, C. F., and Pérez, T.:
675 Climate change effects on a miniature ocean: the highly diverse, highly impacted
676 Mediterranean Sea, Trends Ecol. Evol., 25, 250-260,
677 http://dx.doi.org/10.1016/j.tree.2009.10.009, 2010.

678 Luchetta, A., Cantoni, C., and Catalano, G.: New observations of CO_2-induced acidification
679 in the northern Adriatic Sea over the last quarter century, Chem. Ecol., 26, 1-17,
680 10.1080/02757541003627688, 2010.
681 Lueker, T. J., Dickson, A. G., and Keeling, C. D.: Ocean pCO_2 calculated from dissolved
682 inorganic carbon, alkalinity, and equations for K_1 and K_2: validation based on laboratory
683 measurements of CO_2 in gas and seawater at equilibrium, Mar. Chem., 70, 105-119,
684 10.1016/S0304-4203(00)00022-0, 2000.
685 Macpherson, G. L., Roberts, J. A., Blair, J. M., Townsend, M. A., Fowle, D. A., and Beisner,
686 K. R.: Increasing shallow groundwater CO_2 and limestone weathering, Konza Prairie,
687 USA, Geochim. Cosmochim. Acta, 72, 5581-5599, 10.1016/j.gca.2008.09.004, 2008.
688 Marcellin Yao, K., Marcou, O., Goyet, C., Guglielmi, V., Touratier, F., and Savy, J.-P.: Time
689 variability of the north-western Mediterranean Sea pH over 1995–2011, Mar. Environ.
690 Res., 116, 51-60, 10.1016/j.marenvres.2016.02.016, 2016.
691 McGrath, T., McGovern, E., Cave, R. R., and Kivimäe, C.: The inorganic carbon chemistry
692 in coastal and shelf waters around Ireland, Estuaries and Coasts, 39, 27-39,
693 10.1007/s12237-015-9950-6, 2016.
694 Meier, K. J. S., Beaufort, L., Heussner, S., and Ziveri, P.: The role of ocean acidification in
695 *Emiliania huxleyi* coccolith thinning in the Mediterranean Sea, Biogeosciences, 11, 2857-
696 2869, 10.5194/bg-11-2857-2014, 2014.
697 The MerMex Group, Durrieu de Madron, X., Guieu, C., Sempéré, R., Conan, P., Cossa, D.,
698 D'Ortenzio, F., Estournel, C., Gazeau, F., Rabouille, C., Stemmann, L., Bonnet, S., Diaz,
699 F., Koubbi, P., Radakovitch, O., Babin, M., Baklouti, M., Bancon-Montigny, C., Belviso,
700 S., Bensoussan, N., Bonsang, B., Bouloubassi, I., Brunet, C., Cadiou, J. F., Carlotti, F.,
701 Chami, M., Charmasson, S., Charrière, B., Dachs, J., Doxaran, D., Dutay, J. C., Elbaz-
702 Poulichet, F., Eléaume, M., Eyrolles, F., Fernandez, C., Fowler, S., Francour, P.,

Gaertner, J. C., Galzin, R., Gasparini, S., Ghiglione, J. F., Gonzalez, J. L., Goyet, C., Guidi, L., Guizien, K., Heimbürger, L. E., Jacquet, S. H. M., Jeffrey, W. H., Joux, F., Le Hir, P., Leblanc, K., Lefèvre, D., Lejeusne, C., Lemé, R., Loÿe-Pilot, M. D., Mallet, M., Méjanelle, L., Mélin, F., Mellon, C., Mérigot, B., Merle, P. L., Migon, C., Miller, W. L., Mortier, L., Mostajir, B., Mousseau, L., Moutin, T., Para, J., Pérez, T., Petrenko, A., Poggiale, J. C., Prieur, L., Pujo-Pay, M., Pulido, V., Raimbault, P., Rees, A. P., Ridame, C., Rontani, J. F., Ruiz Pino, D., Sicre, M. A., Taillandier, V., Tamburini, C., Tanaka, T., Taupier-Letage, I., Tedetti, M., Testor, P., Thébault, H., Thouvenin, B., Touratier, F., Tronczynski, J., Ulses, C., Van Wambeke, F., Vantrepotte, V., Vaz, S., and Verney, R.: Marine ecosystems' responses to climatic and anthropogenic forcings in the Mediterranean, Prog. Oceanogr., 91, 97-166, 10.1016/j.pocean.2011.02.003, 2011.

Millot, C., and Taupier-Letage, I.: Circulation in the Mediterranean Sea, in: The Mediterranean Sea, edited by: Saliot, A., Springer Berlin Heidelberg, Berlin, Heidelberg, 29-66, 2005.

Moulin, E., Jordens, A., and Wollast, R.: Influence of the aerobic bacterial respiration on the early dissolution of carbonates in coastal sediments, in: Progress in Belgian Oceanographic Research: Proceedings of a Symposium Held at the Palace of Academies Brussels, edited by: Van Grieken, R., and Wollast, R., Brussels, 196-208, 1985.

Müller, J. D., Schneider, B., and Rehder, G.: Long-term alkalinity trends in the Baltic Sea and their implications for CO_2-induced acidification, Limnol. Oceanogr., 10.1002/lno.10349, 2016.

Oh, N.-H., and Raymond, P. A.: Contribution of agricultural liming to riverine bicarbonate export and CO_2 sequestration in the Ohio River basin, Global Biogeochem. Cycles, 20, GB3012, 10.1029/2005GB002565, 2006.

727 Omstedt, A., Edman, M., Claremar, B., and Rutgersson, A.: Modelling the contributions to
728 marine acidification from deposited SO_x, NO_x, and NH_x in the Baltic Sea: Past and
729 present situations, Cont. Shelf Res., 111, Part B, 234-249, 10.1016/j.csr.2015.08.024,
730 2015.
731 Palmiéri, J., Orr, J., Dutay, J., Béranger, K., Schneider, A., Beuvier, J., and Somot, S.:
732 Simulated anthropogenic CO_2 storage and acidification of the Mediterranean Sea,
733 Biogeosciences, 12, 781-802, 2015.
734 Parravicini, V., Mangialajo, L., Mousseau, L., Peirano, A., Morri, C., Montefalcone, M.,
735 Francour, P., Kulbicki, M., and Bianchi, C. N.: Climate change and warm-water species
736 at the north-western boundary of the Mediterranean Sea, Mar. Ecol., 36, 897-909,
737 10.1111/maec.12277, 2015.
738 Perez, F. F., and Fraga, F.: The pH measurements in seawater on the NBS scale, Mar. Chem.,
739 21, 315-327, 10.1016/0304-4203(87)90054-5, 1987.
740 Pörtner, H.-O., Karl, D., Boyd, P. W., Cheung, W., Lluch-Cota, S. E., Nojiri, Y., Schmidt, D.
741 N., and Zavialov, P.: Ocean systems, in: Climate Change 2014: Impacts, Adaptation, and
742 Vulnerability. Part A: Global and Sectoral Aspects. Contribution of Working Group II to
743 the Fifth Assessment Report of the Intergovernmental Panel on Climate Change, edited
744 by: Field, C. B., Barros, V. R., Dokken, D. J., Mach, K. J., Mastrandrea, M. D., Bilir, T.
745 E., Chatterjee, M., Ebi, K. L., Estrada, Y. O., Genova, R. C., Girma, B., Kissel, E. S.,
746 Levy, A. N., MacCracken, S., Mastrandrea, P. R., and L.L.White, Cambridge University
747 Press, Cambridge, United Kingdom and New York, NY, USA, 411-484, 2014.
748 Provoost, P., van Heuven, S., Soetaert, K., Laane, R. W. P. M., and Middelburg, J. J.:
749 Seasonal and long-term changes in pH in the Dutch coastal zone, Biogeosciences, 7,
750 3869-3878, 10.5194/bg-7-3869-2010, 2010.

751 Raymond, P. A., and Cole, J. J.: Increase in the export of alkalinity from North America's
752 largest river, Science, 301, 88-91, 2003.
753 Rhein, M., Rintoul, S. R., Aoki, S., Campos, E., Chambers, D., Feely, R. A., Gulev, S.,
754 Johnson, G. C., Josey, S. A., A. Kostianoy, Mauritzen, C., Roemmich, D., Talley, L. D.,
755 and Wang, F.: Observations: Ocean, in: Climate Change 2013: The Physical Science
756 Basis. Contribution of Working Group I to the Fifth Assessment Report of the
757 Intergovernmental Panel on Climate Change, edited by: Stocker, T. F., Qin, D., Plattner,
758 G.-K., Tignor, M., Allen, S. K., Boschung, J., Nauels, A., Xia, Y., Bex, V., and Midgley,
759 P. M., Cambridge University Press, Cambridge, United Kingdom and New York, NY,
760 USA., 2013.
761 Schneider, A., Wallace, D. W. R., and Körtzinger, A.: Alkalinity of the Mediterranean Sea,
762 Geophys. Res. Lett., 34, L15608, 10.1029/2006GL028842, 2007.
763 Schneider, A., Tanhua, T., Körtzinger, A., and Wallace, D. W. R.: High anthropogenic
764 carbon content in the eastern Mediterranean, J. Geophys. Res., 115, C12050,
765 10.1029/2010JC006171, 2010.
766 Slomp, C. P., and Van Cappellen, P.: Nutrient inputs to the coastal ocean through submarine
767 groundwater discharge: controls and potential impact, Journal of Hydrology, 295, 64-86,
768 10.1016/j.jhydrol.2004.02.018, 2004.
769 Stets, E. G., Kelly, V. J., and Crawford, C. G.: Long-term trends in alkalinity in large rivers
770 of the conterminous US in relation to acidification, agriculture, and hydrologic
771 modification, Sci. Total Environ., 488–489, 280-289, 10.1016/j.scitotenv.2014.04.054,
772 2014.
773 Tamše, S., Ogrinc, N., Walter, L. M., Turk, D., and Faganeli, J.: River sources of dissolved
774 inorganic carbon in the Gulf of Trieste (N Adriatic): stable carbon isotope evidence,
775 Estuaries and Coasts, 38, 151-164, 10.1007/s12237-014-9812-7, 2015.

776 Tanhua, T., Bates, N. R., and Körtzinger, A.: The marine carbon cycle and ocean
777 anthropogenic CO_2 inventories, in: Ocean Circulation and Climate: A 21st Century
778 Perspective. 2nd Ed, edited by: Siedler, G., Griffies, S., Gould, J., and Church, J., 103,
779 Academic Press, 787-816, 2013.
780 Team, R. C.: R: A language and environment for statistical computing. R Foundation for
781 Statistical Computing, Vienna, Austria. https://www.r-project.org/, 2016.
782 Touratier, F., and Goyet, C.: Impact of the Eastern Mediterranean Transient on the
783 distribution of anthropogenic CO_2 and first estimate of acidification for the Mediterranean
784 Sea, Deep-Sea Res. I, 58, 1-15, 10.1016/j.dsr.2010.10.002, 2011.
785 Touratier, F., Goyet, C., Houpert, L., de Madron, X. D., Lefèvre, D., Stabholz, M., and
786 Guglielmi, V.: Role of deep convection on anthropogenic CO_2 sequestration in the Gulf
787 of Lions (northwestern Mediterranean Sea), Deep-Sea Res. I, 113, 33-48,
788 10.1016/j.dsr.2016.04.003, 2016.
789 Vargas, C. A., Contreras, P. Y., Pérez, C. A., Sobarzo, M., Saldías, G. S., and Salisbury, J.:
790 Influences of riverine and upwelling waters on the coastal carbonate system off Central
791 Chile and their ocean acidification implications, Journal of Geophysical Research:
792 Biogeosciences, 121, 1468-1483, 10.1002/2015JG003213, 2016.
793 Wolf-Gladrow, D. A., Zeebe, R. E., Klaas, C., Körtzinger, A., and Dickson, A. G.: Total
794 alkalinity: The explicit conservative expression and its application to biogeochemical
795 processes, Mar. Chem., 106, 287-300, 10.1016/j.marchem.2007.01.006, 2007.
796 Wootton, J. T., Pfister, C. A., and Forester, J. D.: Dynamic patterns and ecological impacts of
797 declining ocean pH in a high-resolution multi-year dataset, Proc. Natl. Acad. Sci., 105,
798 18848-18853, 2008.
799 Wootton, J. T., and Pfister, C. A.: Carbon system measurements and potential climatic
800 drivers at a site of rapidly declining ocean pH, PLoS One, 7, e53396, 2012.

Table 1. Previous estimates or documentation of pH change (ΔpH**)** in the Mediterranean Sea. 'Total' indicates estimates made for the whole Mediterranean Sea. TrOCA is the 'Tracer combining Oxygen, inorganic Carbon, and total Alkalinity' method, NR means 'not reported', and PI is 'pre-industrial era'. *indicates studies where the reported pH change was assumed to be at *in situ* temperatures.

Region	***Site***	***Method***	***Study period***	***pH scale***	***°C***	***ΔpH yr^{-1} ± SE***	***Total ΔpH***	***Reference***
NW	Point B, 1 m	time-series, anomaly	2007-2015	total	*in situ*	-0.0028 ± 0.0003	-0.0252	This study
NW	Point B, 1 m	time-series, anomaly	2007-2015	total	25	-0.0017 ± 0.0002	-0.0153	This study
NW	Point B	model	1967-2003	total	*in situ*	-0.0014	-0.05	Howes et al. (2015)
NW	DYFAMED	time-series, observed	1995-2011	seawater	*in situ*	-0.003 ± 0.001	-0.051	Marcellin Yao et al. (2016)
NW	DYFAMED	time-series comparison	1998-2000, 2003-2005	seawater	*in situ**	-	-0.02	Meier et al. (2014)
NW	Gulf of Lion	TrOCA	PI-2011	NR	*in situ**	-	-0.15 to -0.11	Touratier et al. (2016)
East	N Adriatic Sea	cruise comparison	1983, 2008	total	25	-0.0025	-0.063	Luchetta et al. (2010)
East	Otranto Strait	TrOCA	PI-1995	seawater	25	-	< -0.1 to -0.05, ± 0.014	Krasakopoulou et al. (2011)
Total	Full profile	TrOCA	PI-2001	NR	*in situ**	-	-0.14 to -0.05	Touratier and Goyet (2011)
Total	Bottom waters	model	1800-2001	total	*in situ**	-	-0.06 to -0.005	Palmiéri et al. (2015)
Total	Surface waters	model	1800-2001	total	*in situ**	-	-0.084 ± 0.001	Palmiéri et al. (2015)
Gibraltar Strait	Espartel sill	pH, pCO_2 sensors	2012-2015	total	25	-0.0044 ± 0.00006	-	Flecha et al. (2015)

Table 2. Time-series anomaly regression analyses on seawater carbonate chemistry at Point B for salinity (S), temperature (T), dissolved inorganic carbon (C_T), total alkalinity (A_T), pH_T, pH_T normalized to 25 ºC (pH_{T25}), pCO_2, calcite (Ω_c) and aragonite (Ω_a) saturation state, and salinity-normalized A_T (nA_T) and C_T (nC_T), at 1 and 50 m. Slopes represent the change in the variable unit per year. P <<0.001 indicates p-values far smaller than 0.001.

Depth (m)	*Variable*	*Slope ± SE*	*Intercept ± SE*	*N*	*F*	*df*	*Slope P*	R^2
1	S	-0.0017 ± 0.0044	3.38 ± 8.82	417	0.147	1,415	0.702	0
	T (ºC)	0.072 ± 0.022	-145 ± 44	413	10.999	1,411	0.001	0.026
	C_T (µmol kg^{-1})	2.97 ± 0.20	-5965 ± 400	416	221.87	1,414	<<0.001	0.349
	A_T (µmol kg^{-1})	2.08 ± 0.19	-4189 ± 379	417	122.429	1,415	<<0.001	0.228
	pH_T	-0.0028 ± 0.0003	5.72 ± 0.66	412	74.205	1,410	<<0.001	0.153
	pH_{T25}	-0.0017 ± 0.0002	3.46 ± 0.43	412	64.204	1, 410	<<0.001	0.1354
	pCO_2 (µatm)	3.53 ± 0.39	-7105 ± 776	412	83.927	1,410	<<0.001	0.17
	Ω_c	-0.0109 ± 0.0022	22.0 ± 4.5	412	24.08	1,410	<<0.001	0.055
	Ω_a	-0.0064 ± 0.0015	12.9 ± 3.1	412	17.33	1,410	<<0.001	0.041
	nA_T (µmol kg^{-1})	2.20 ± 0.28	-4425 ± 560	412	62.34	1,410	<<0.001	0.132
	nC_T (µmol kg^{-1})	3.12 ± 0.29	-6275 ± 579	412	117.486	1,410	<<0.001	0.223
50	S	0.0063 ± 0.0020	-12.8 ± 4.1	412	9.858	1, 410	0.002	0.0235
	T (ºC)	0.088 ± 0.019	-177 ± 38	408	21.927	1, 406	<<0.001	0.0512
	C_T (µmol kg^{-1})	2.16 ± 0.21	-4344 ± 418	411	108.105	1, 409	<<0.001	0.2091
	A_T (µmol kg^{-1})	1.59 ± 0.15	-3192 ± 309	412	106.947	1, 410	<<0.001	0.2069
	pH_T	-0.0026 ± 0.0002	5.28 ± 0.50	407	112.111	1, 405	<<0.001	0.2168
	pH_{T25}	-0.0013 ± 0.0003	2.55 ± 0.54	407	21.863	1, 405	<<0.001	0.0512
	pCO_2 (µatm)	2.79 ± 0.25	-5603 ± 501	407	125.1	1, 405	<<0.001	0.236
	Ω_c	-0.0070 ± 0.0027	14.0 ± 5.4	407	6.648	1, 405	0.01	0.0162
	Ω_a	-0.0038 ± 0.0019	7.6 ± 3.7	407	4.155	1, 405	0.042	0.0102
	nA_T (µmol kg^{-1})	1.15 ± 0.13	-2309 ± 254	407	82.309	1, 405	<<0.001	0.1689
	nC_T (µmol kg^{-1})	1.82 ± 0.19	-3661 ± 376	407	94.98	1, 405	<<0.001	0.19

815 **Table 3.** Deconvolution of pH_T anomalies ($\frac{dpH_T}{dt}$, units pH_T yr^{-1}) at 1 and 50 m.

816 Sensitivity of pH_T with respect to variables ($\frac{\partial pH_T}{\partial var}$), where the variable *var* is either

817 temperature (T), salinity (S), total alkalinity (A_T), or dissolved inorganic carbon (C_T), was

818 multiplied by the anomaly of *var* ($\frac{dT}{dt}$, Table 2). SE is standard error and RMSE is root-mean-

819 squared error. Rounding was performed at the end of the calculations, prior to estimating

820 percent contributions.

Depth (m)	***var***	$\frac{\partial pH_T}{\partial var}$ ± ***SE***	$\frac{\partial pH_T}{\partial var}\frac{dvar}{dt}$ ± ***RMSE***	***Contribution (%)***	$\frac{dpH_T}{dt}$ ± ***RMSE***
1	T (ºC)	-0.0153 ± <0.0001	-0.0011 ± 0.0003	41	-0.0027 ± 0.0005
	S	-0.0117 ± <0.0001	<0.0001 ± 0.0001	0	
	A_T (µmol kg^{-1})	0.0015 ± <0.0001	0.0031 ± 0.0003	-115	
	C_T (µmol kg^{-1})	-0.0016 ± <0.0001	-0.0047 ± 0.0003	174	
50	T (ºC)	-0.0154 ± <0.0001	-0.0014 ± 0.0003	54	-0.0026 ± 0.0005
	S	-0.0116 ± <0.0001	-0.0001 ± <0.0001	4	
	A_T (µmol kg^{-1})	0.0015 ± <0.0001	0.0024 ± 0.0002	-92	
	C_T (µmol kg^{-1})	-0.0016 ± <0.0001	-0.0035 ± 0.0003	135	

821

Table 4. Deconvolution of pCO_2 anomalies ($\frac{dpCO_2}{dt}$, µatm yr^{-1}) at 1 and 50 m. Details are the same as in Table 3.

Depth (m)	*var*	$\frac{\partial pH_T}{\partial var}$ ± *SE*	$\frac{\partial pH_T}{\partial var}\frac{dvar}{dt}$ ± *RMSE*	*Contribution (%)*	$\frac{dpH_T}{dt}$ ± *RMSE*
1	T (ºC)	16.49 ± 0.05	1.19 ± 0.36	37	3.23 ± 0.57
	S	10.14 ± <0.01	-0.02 ± 0.05	-1	
	A_T (µmol kg^{-1})	-1.478 ± 0.005	-3.08 ± 0.28	-95	
	C_T (µmol kg^{-1})	1.735 ± 0.006	5.14 ± 0.35	159	
50	T (ºC)	15.55 ± 0.03	1.37 ± 0.29	48	2.84 ± 0.49
	S	9.355 ± <0.001	0.06 ± 0.02	2	
	A_T (µmol kg^{-1})	-1.327 ± 0.002	-2.11 ± 0.20	-74	
	C_T (µmol kg^{-1})	1.629 ± 0.005	3.52 ± 0.34	124	

825 **Figure 1.** Map of study region in the NW Mediterranean Sea (a), along the North current (b)
826 in the Bay of Villefranche-sur-Mer, France (c). Point B station, EOL buoy, and the offshore
827 time-series station DYFAMED are marked. Bathymetric line units are m (c).

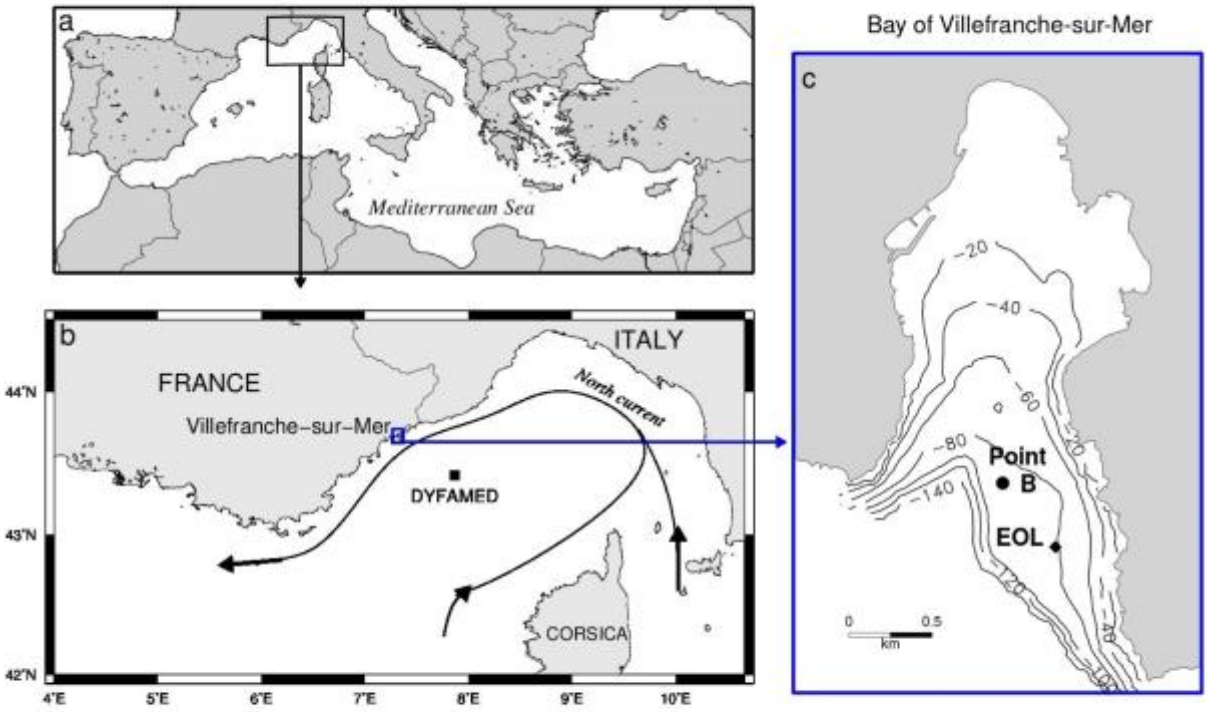

828

Figure 2. Time-series observations (a-g) and anomaly trends (h-n) for temperature, salinity, and seawater carbonate chemistry at Point B, 1 m. Regression slopes are drawn ± SE (in grey) and noted with a star for significance at $\alpha = 0.05$.

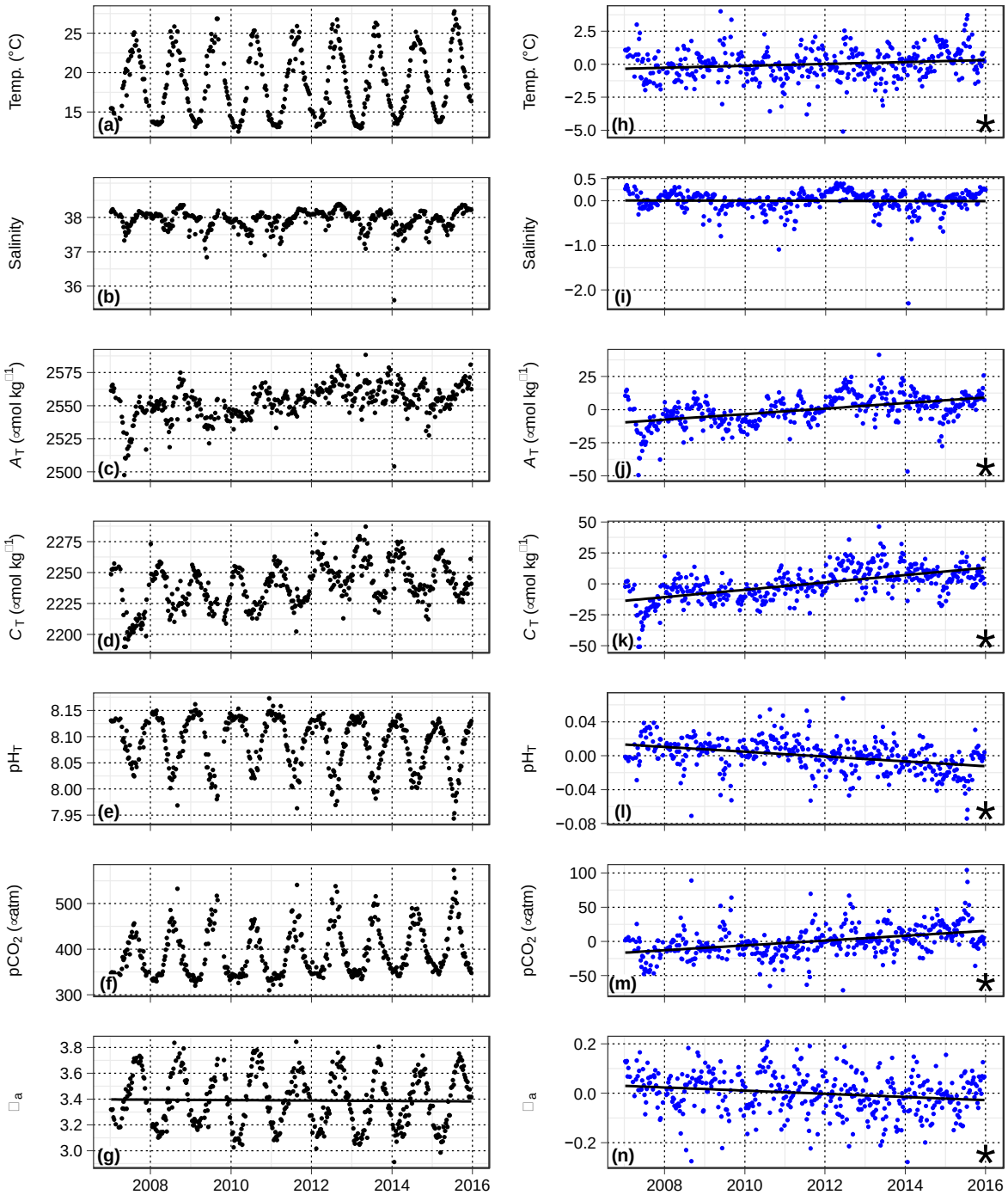

Figure 3. Time-series observations (a-g) and anomaly trends (h-n) for temperature, salinity, and seawater carbonate chemistry at Point B, 50 m. Regression slopes are drawn ± SE (in grey) and noted with a star for significance at $\alpha = 0.05$.

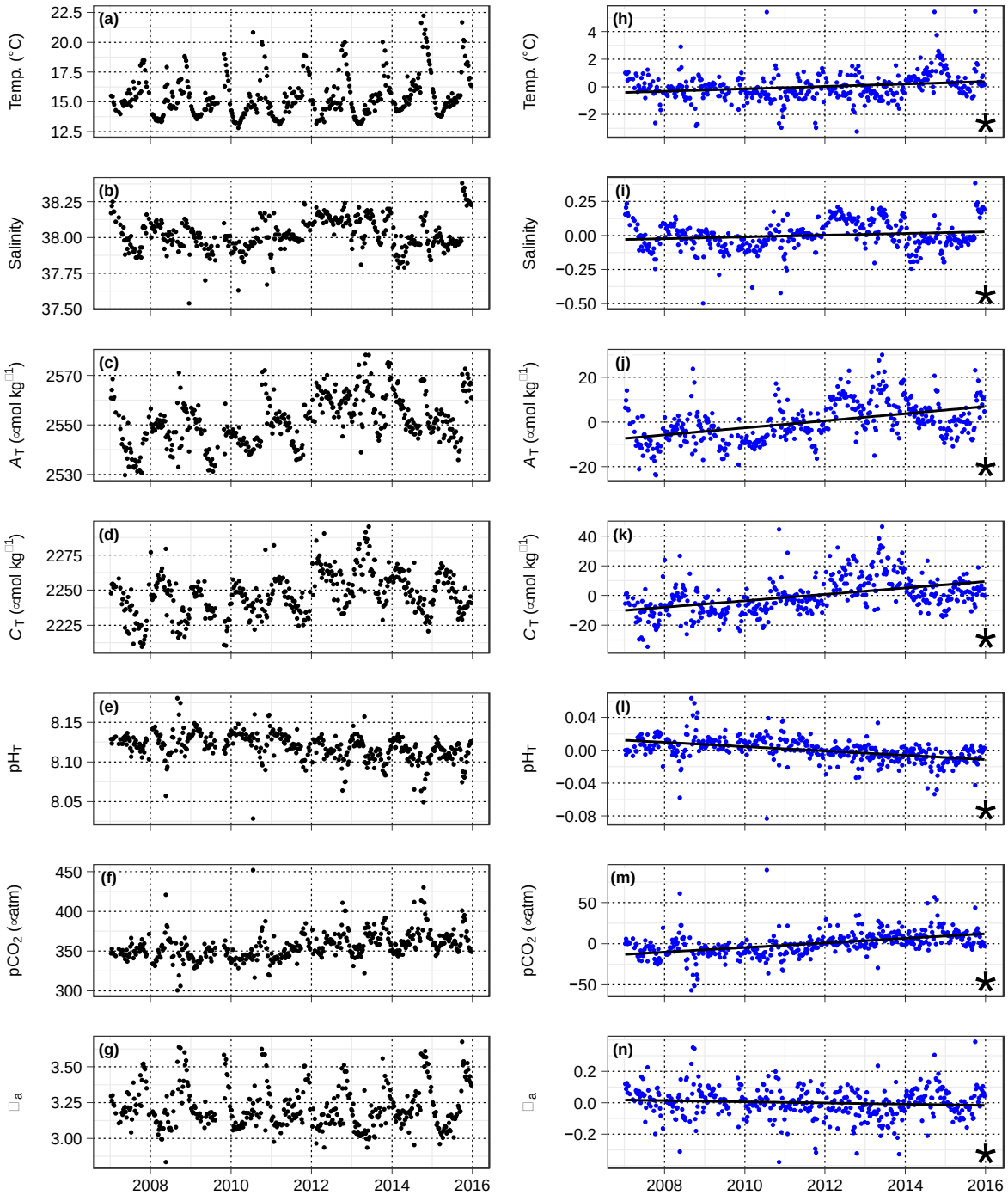

Figure 4. Monthly distribution of seawater carbonate chemistry at Point B, 1 m, using a combination of a violin plot showing the relative frequency of the observations (shaded blue area) and a boxplot showing the median, first and third quartiles, as well as outliers (blue).

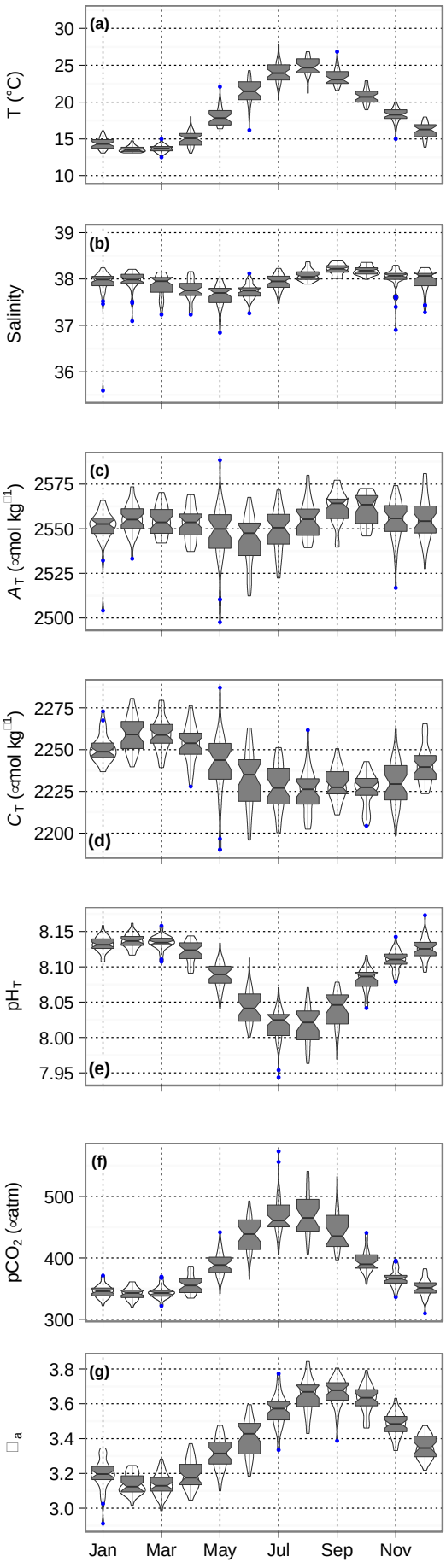

844 **Figure 5.** Monthly trends of total alkalinity (A_T, blue) and dissolved inorganic carbon (C_T,

845 green) for the period 2007-2015. Errors bars are ± SE of the slope estimate and significance

846 is noted (*) at α=0.05.

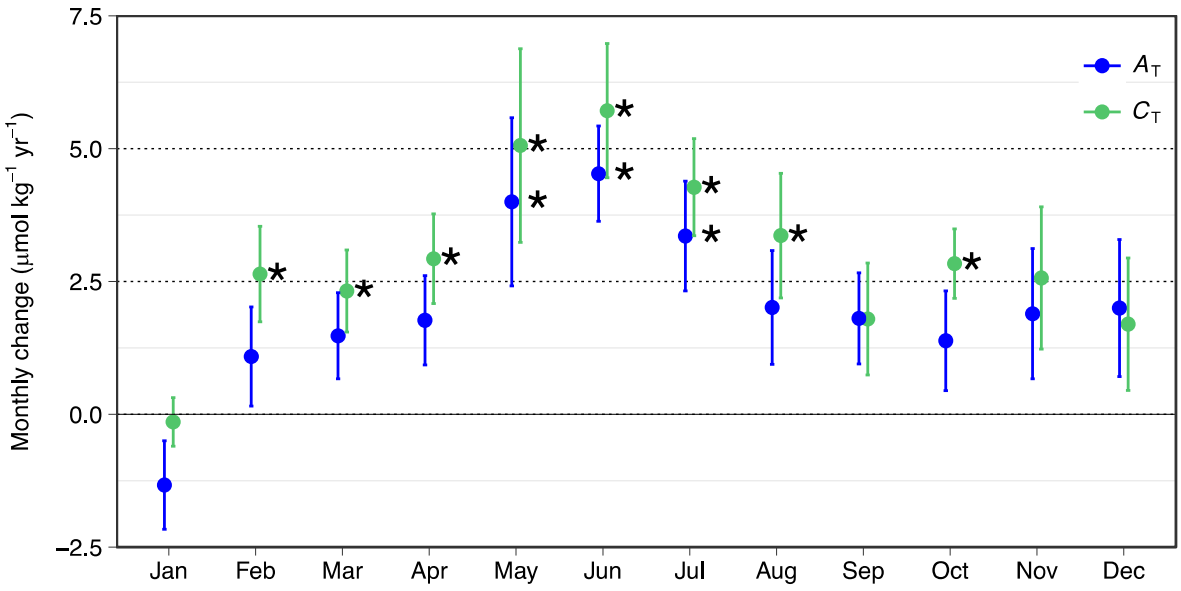

847

Figure 6. Salinity and total alkalinity relationships at Point B for the period 2007-2015, by year, at 1 m. Data points are colored for month.

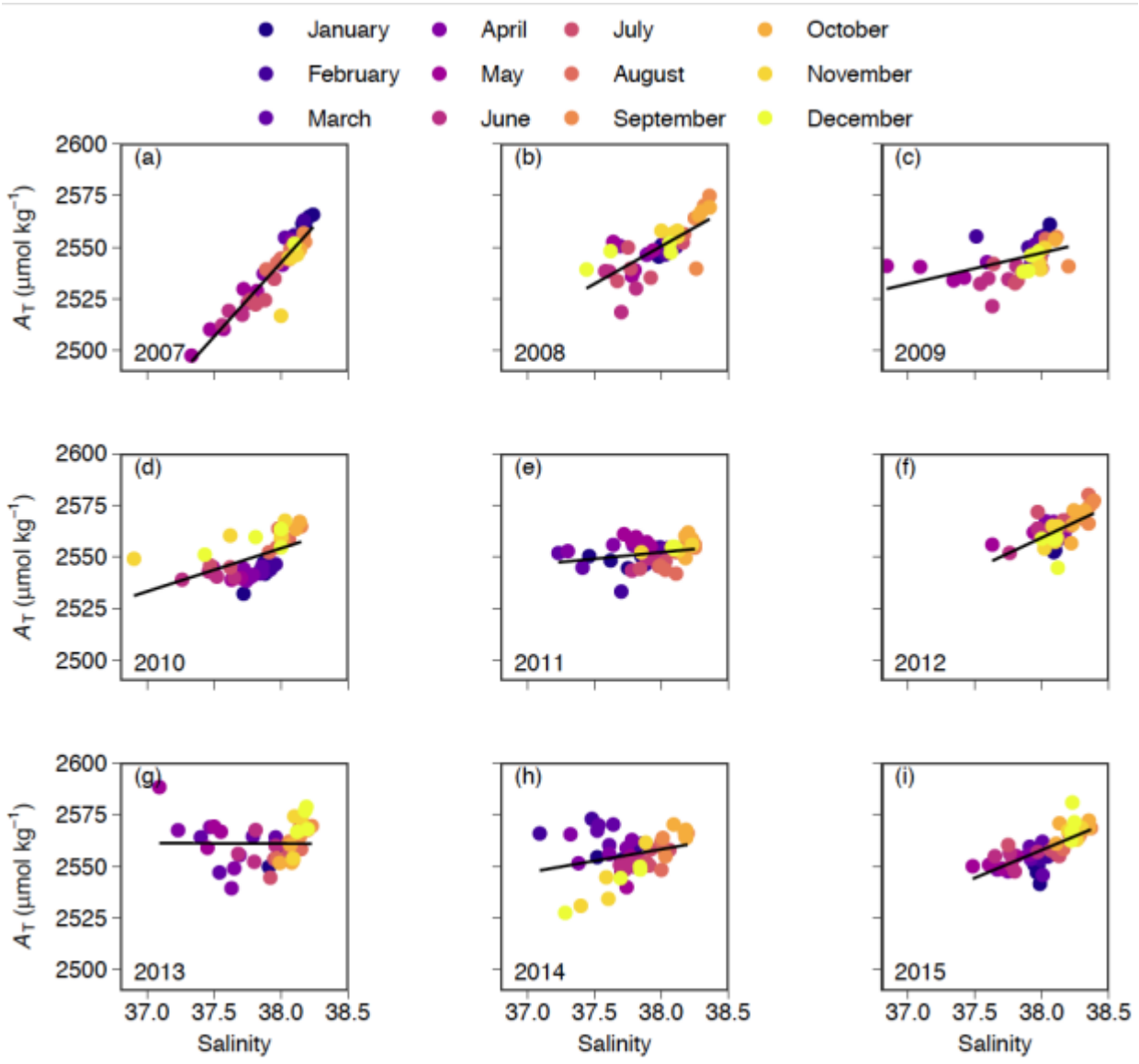

Figure 7. Time-series pH (a) and temperature (b) from autonomous SeaFET pH sensor deployments at EOL buoy, 2 m. Discrete calibration samples are noted in green, and grey vertical lines bracket deployment periods (a). Calibration sample offsets from processed pH time-series are shown in panel (c). Violin and boxplots (see Fig. 4) show diel pH range by month (d), and an example of this pH variability is shown for May 2015 (e).